Surface Cauchy-Born analysis of surface stress effects on metallic nanowires

Harold S. Park[1,*] and Patrick A. Klein[2]

[1]*Department of Civil and Environmental Engineering, Vanderbilt University, Nashville, Tennessee 37235, USA*
[2]*Franklin Templeton Investments, San Mateo, California 94403, USA*
(Received 25 September 2006; revised manuscript received 28 November 2006; published 7 February 2007)

We present a surface Cauchy-Born approach to modeling FCC metals with nanometer scale dimensions for which surface stresses contribute significantly to the overall mechanical response. The model is based on an extension of the traditional Cauchy-Born theory in which a surface energy term that is obtained from the underlying crystal structure and governing interatomic potential is used to augment the bulk energy. By doing so, solutions to three-dimensional nanomechanical boundary value problems can be found within the framework of traditional nonlinear finite element methods. The major purpose of this work is to utilize the surface Cauchy-Born model to determine surface stress effects on the minimum energy configurations of single crystal gold nanowires using embedded atom potentials on wire sizes ranging in length from 6 to 280 nm with square cross sectional lengths ranging from 6 to 35 nm. The numerical examples clearly demonstrate that other factors beside surface area to volume ratio and total surface energy minimization, such as geometry and the percentage of transverse surface area, are critical in determining the minimum energy configurations of nanowires under the influence of surface stresses.

I. INTRODUCTION

The recent explosion of interest in sustainable nanotechnologies has driven the development and discovery of nanomaterials. Many different nanoscale structural elements have been studied and synthesized; examples of these include carbon nanotubes,[1] nanowires,[2–4] nanoparticles,[5,6] and quantum dots.[7] Because of their nanometer scale dimensions, these materials are characterized by having a relatively large ratio of surface area to volume. The large surface area to volume ratio combined with nanoscale confinement effects causes these nanomaterials to exhibit physical properties, i.e., optical, mechanical, electrical, and thermal, that can be dramatically different from those seen in the corresponding bulk materials.[4]

In analyzing the mechanical behavior of nanomaterials, a key feature of interest is intrinsic surface stresses that arise due to their large exposed surface areas.[8] Surface stresses have recently been found to cause phase transformations in gold nanowires,[9] self-healing behavior in metal nanowires,[10–12] and surface reorientations in thin metallic films and wires.[13,14] Surface and confinement effects are also known to cause elevated strength in nanomaterials,[15–18] orientation-dependent surface elastic properties[19–21] and a first-order effect on the operant modes of inelastic deformation in metal nanowires.[22]

The size-dependent elastic behavior of nanomaterials has resulted in an increasing amount of literature describing continuum approaches.[8,20,23–32] A common thread that connects some of the above works[25,27,28] is that they are based on modifications to the surface elasticity formulation of Gurtin and Murdoch,[23] in which a surface stress tensor is introduced to augment the bulk stress tensor typically utilized in continuum mechanics. A complicating factor in this formulation is due to the presence of the surface stress, which creates a coupled system of equations with nonstandard boundary conditions. The solution of the coupled field equations combined with the nonclassical boundary conditions makes the application of this theory to generalized boundary value problems a challenging task. Furthermore, very few if any computational models have been developed that can capture the coupled effects of surface stress, size, and geometry on realistic three-dimensional FCC metal nanostructures.

Alternatively, multiple scale models of nanomaterials have been developed to combine the insights into the detailed response of materials that are available through atomistics with the reduced computational expense that continuum approaches offer. Methods for both quasistatic[33–36] and dynamic coupling of atomistics and continua[37–46] have been proposed. With few exceptions,[36] a critical issue with these methods is that the continuum region generally surrounds or encloses the atomistic region, thereby eliminating the effects of surface stresses on the atomistic behavior.

Therefore, the motivation for the present work is the representation of the total energy of a body that obtains the bulk and surface portions directly from atomistic principles, enables an easy discretization using standard nonlinear finite element (FE) techniques,[47] and can be used to predict the size and surface stress-dependent mechanical behavior of three-dimensional FCC metal nanostructures. We accomplish this by building upon previous developments for pair potentials[48] in which the system potential energy is decomposed into bulk and surface components; while this decomposition has been considered before,[8,23,30] those works require either higher order terms in the surface energy or empirical fits to constants for the surface stress which require additional atomistic simulations. In contrast, the uniqueness of the present approach is that the surface energies are obtained using ideas relevant to Cauchy-Born (CB) constitutive modeling.[33,49,50]

By utilizing the CB hypothesis to define the surface energy density, a potential energy that is comprised of both surface and bulk contributions can be constructed, then minimized numerically using standard nonlinear FE techniques while the surface stress effects are transferred naturally to the computational model. Numerical examples are shown directly comparing results obtained using the proposed surface CB model for surface-stress-driven relaxation of gold nano-

wires using embedded atom method (EAM) (Ref. [51]) potentials to fully atomistic simulations; additional examples explore the effects of the surface area to volume ratio and geometry on the surface stress influenced minimum energy configurations of gold nanowires.

II. SURFACE CAUCHY-BORN FORMULATION FOR THE EMBEDDED ATOM METHOD

A. Brief overview of Cauchy-Born theory

The CB rule is a hierarchical multiscale assumption that enables the calculation of continuum stress and moduli from atomistic principles.[33] In this work, we will focus on applying the CB rule to FCC metals whose behavior can be well represented using EAM potentials;[51] the CB assumption has recently been extended to study carbon nanotubes[50,52] as well as semiconductors such as silicon.[53] Considering a purely atomistic system, the EAM energy for an atom U_i is written as

$$U_i = F_i(\bar{\rho}_i) + \frac{1}{2}\sum_{j \neq i}^{nb_i} \phi_{ij}(r_{ij}), \qquad (1)$$

$$\bar{\rho}_i = \sum_{j \neq i}^{nb_i} \rho_j(r_{ij}), \qquad (2)$$

where nb_i are the number of bonds of atom i, F_i is the embedding function, $\bar{\rho}_i$ is the total electron density at atom i, ρ_j is the contribution to the electron density at atom i from atom j, ϕ_{ij} is a pair interaction function and r_{ij} is the distance between atoms i and j. We note that the number of bonds nb_i is dictated by the cutoff distance of the interatomic potential.

In order to turn the atomistic potential energy into a form suitable for the CB approximation, two steps are taken. First, the potential energy is converted into a strain energy density through normalization by a representative atomic volume Ω_0; Ω_0 can be calculated noting that there are four atoms in an FCC unit cell of volume a_0^3, where a_0 is the lattice parameter. Thus $\Omega_0 = 4/a_0^3$ for a $\langle 100 \rangle$ oriented crystal. Second, the neighborhood surrounding each atom is constrained to deform homogeneously via continuum mechanics quantities such as the deformation gradient $\mathbf{F}$, or the stretch tensor $\mathbf{C} = \mathbf{F}^T \mathbf{F}$. The resulting EAM strain energy density Φ is

$$\Phi(\mathbf{C}) = \frac{1}{2\Omega_0}\sum_{j \neq i}^{nbrv_i} (F_i\{\bar{\rho}_i[r_{ij}(\mathbf{C})]\} + \phi_{ij}[r_{ij}(\mathbf{C})]), \qquad (3)$$

where $nbrv_i$ are the number of bonds in the representative unit volume for atom i. For homogeneous deformations, integrating the CB strain energy in Eq. (3) over the representative volume Ω_0 gives the same result as the energy of an atomic unit cell in a homogeneously deforming crystal. This energetic equivalence forms the basis of the traditional CB hypothesis, in which lattice defects are not allowed; other works, notably the quasicontinuum method,[33] have been developed to relieve this restriction. Once the strain energy density is known, continuum stress measures such as the second Piola-Kirchoff stress $\mathbf{S}$, which can be interpreted as

the actual force mapped to the undeformed configuration divided by the undeformed area,[47] can be defined as

$$\mathbf{S} = 2\frac{\partial \Phi(\mathbf{C})}{\partial \mathbf{C}} = \frac{1}{\Omega_0}\frac{\partial U(\mathbf{C})}{\partial \mathbf{r}}\frac{\partial \mathbf{r}}{\partial \mathbf{C}}, \qquad (4)$$

while the material tangent modulus $\mathcal{C}$ is defined to be

$$\mathcal{C} = 2\frac{\partial \mathbf{S}}{\partial \mathbf{C}}. \qquad (5)$$

Another key restriction of the CB hypothesis that motivated the present work is that all points are assumed to lie in the bulk as $\Phi(\mathbf{C})$ does not account for surface effects. Therefore, the issue at hand is to develop an expression for the energy density along the surfaces of a body, where the potential energy of atoms differs from the bulk due to undercoordination; here, undercoordination is used to describe the fact that atoms at the surfaces of a material have fewer bonding neighbors than atoms that lie within the bulk portion of the material. We will describe in the next section how surface effects can be included using the CB assumption.

B. Surface Cauchy-Born extension for embedded atom method

In this section, we discuss the methodology by which the energy density of a body can be represented using the CB assumption with appropriate modifications for the surface energy contributions; further details can be found in earlier work by the authors.[48] The relationship between the continuum strain energy density and the total potential energy of the corresponding, defect-free atomistic system can be written as

$$\sum_{i=1}^{natoms} U_i(r) = \int_{\Omega_0^{bulk}} \Phi(\mathbf{C})d\Omega + \int_{\Gamma_0} \gamma(\mathbf{C})d\Gamma, \qquad (6)$$

where r is the interatomic distance, $\Phi(\mathbf{C})$ is the bulk strain energy density, Ω_0^{bulk} represents the volume of the body in which all atoms are fully coordinated, $\gamma(\mathbf{C})$ is the surface strain energy density, Γ_0 represents the surface area of the body in which the atoms are undercoordinated and *natoms* is the total number of atoms in the system.

As discussed in the introduction, most surface elastic models decompose the total energy of the continuum body into surface and bulk contributions. The uniqueness of the present approach is the usage of the CB approximation in constructing the surface energy density; we now discuss how the CB approximation can be utilized to approximate the surface energy density.

We first note that for $\langle 100 \rangle$ FCC crystals whose interactions are governed by EAM potentials, there exist four nonbulk layers of atoms at the surfaces, as illustrated in Fig. 1. Thus, we rewrite Eq. (6) taking into account the four nonbulk layers to read
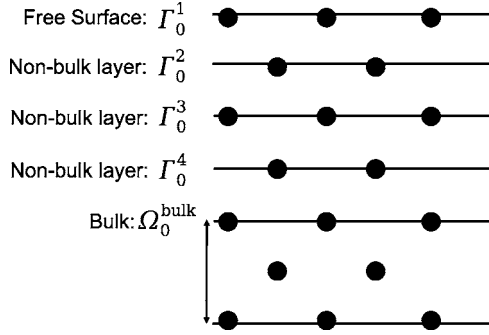
FIG. 1. Illustration of bulk and nonbulk layers of atoms in a $\langle 100 \rangle$ FCC crystal with $\{100\}$ surfaces interacting by an EAM potential.

$$\sum_{i}^{natoms} U_i(r) = \int_{\Omega_0^{\text{bulk}}} \Phi(\mathbf{C})d\Omega + \int_{\Gamma_0^1} \gamma_{\Gamma_0^1}(\mathbf{C})d\Gamma + \int_{\Gamma_0^2} \gamma_{\Gamma_0^2}(\mathbf{C})d\Gamma$$
$$+ \int_{\Gamma_0^3} \gamma_{\Gamma_0^3}(\mathbf{C})d\Gamma + \int_{\Gamma_0^4} \gamma_{\Gamma_0^4}(\mathbf{C})d\Gamma. \quad (7)$$

Having defined the energy equivalence including both bulk and surface effects, we now determine the surface energy densities $\gamma(\mathbf{C})$. Analogous to the bulk energy density, the surface energy densities $\gamma(\mathbf{C})$ will describe the energy per representative undeformed *area* of atoms at or near the surface of a homogeneously deforming crystal. For FCC metals, choosing a surface unit cell that contains only one atom is sufficient to reproduce the structure of each surface layer. The surface unit cell possesses translational symmetry only in the plane of the surface, unlike the bulk unit cell which possesses translational symmetry in all directions. Thus, the surface energy density for a representative atom in a given surface layer in Fig. 1 can be written generally as

$$\gamma_{\Gamma_0^a}(\mathbf{C}) = \frac{1}{2\Gamma_0^a} \sum_{j \neq i}^{nb_a} (F_i\{\bar{\rho}_i[r_{ij}(\mathbf{C})]\} + \phi_{ij}[r_{ij}(\mathbf{C})]), \quad (8)$$

where Γ_0^a is the area occupied by an atom in surface layer a and nb_a are the number of bonds for an atom in surface layer a; the number of bonds nb_a is dictated by the range of the interatomic potential such that each representative surface atom has the same bonding environment as the equivalent surface atom in a fully atomistic calculation.

We note in closing this section that because we have assumed that the energetics of each surface layer can be described by a single representative atom, we have ignored the effects of edge and corner atoms. While these atoms are expected to play an important role in truly small nanostructures,[54] the system size at which these effects become significant can easily be described using direct molecular calculations. As will be demonstrated in the numerical examples, the current methodology is geared for larger problems where such edge and corner effects are relatively insignificant, and simultaneously where the system size for fully atomistic calculations becomes prohibitive.

C. Finite element approximation

Having defined the surface energy densities $\gamma(\mathbf{C})$ for each nonbulk layer of atoms near the surface, we can immediately write the total potential energy Π of the system including external loads $\mathbf{T}$ as

$$\Pi(\mathbf{u}) = \int_{\Omega_0^{\text{bulk}}} \Phi(\mathbf{C})d\Omega + \int_{\Gamma_0^1} \gamma_{\Gamma_0^1}(\mathbf{C})d\Gamma + \int_{\Gamma_0^2} \gamma_{\Gamma_0^2}(\mathbf{C})d\Gamma$$
$$+ \int_{\Gamma_0^3} \gamma_{\Gamma_0^3}(\mathbf{C})d\Gamma + \int_{\Gamma_0^4} \gamma_{\Gamma_0^4}(\mathbf{C})d\Gamma - \int_{\Gamma_0} (\mathbf{T} \cdot \mathbf{u})d\Gamma. \quad (9)$$

In order to obtain a form suitable for FE calculations, we introduce the standard discretization of the displacement field $\mathbf{u}(\mathbf{X})$ using FE shape functions as

$$\mathbf{u}(\mathbf{X}) = \sum_{I=1}^{nn} N_I(\mathbf{X})\mathbf{u}_I, \quad (10)$$

where N_I are the shape or interpolation functions, nn are the total number of nodes in the discretized continuum, and $\mathbf{u}_I$ are the displacements of node I.[47,55] Substituting Eqs. (3) and (8) into Eq. (9) and differentiating gives the minimizer of the potential energy and also the FE nodal force balance[47]

$$\frac{\partial \Pi}{\partial \mathbf{u}_I} = \int_{\Omega_0^{\text{bulk}}} \mathbf{B}^T \mathbf{S} \mathbf{F}^T d\Omega + \int_{\Gamma_0^1} \mathbf{B}^T \widetilde{\mathbf{S}}^{(1)} \mathbf{F}^T d\Gamma + \int_{\Gamma_0^2} \mathbf{B}^T \widetilde{\mathbf{S}}^{(2)} \mathbf{F}^T d\Gamma$$
$$+ \int_{\Gamma_0^3} \mathbf{B}^T \widetilde{\mathbf{S}}^{(3)} \mathbf{F}^T d\Gamma + \int_{\Gamma_0^4} \mathbf{B}^T \widetilde{\mathbf{S}}^{(4)} \mathbf{F}^T d\Gamma - \int_{\Gamma_0} N_I \mathbf{T} d\Gamma, \quad (11)$$

where $\mathbf{S}$ is the second Piola-Kirchoff stress due to the bulk strain energy and $\mathbf{B}^T = \left(\frac{\partial N_I}{\partial \mathbf{X}}\right)^T$; $\widetilde{\mathbf{S}}^{(a)}$ can be loosely labeled as surface Piola-Kirchoff stresses on layer a that can be found using Eqs. (8) and (4) to be of the form

$$\widetilde{\mathbf{S}}^{(a)}(\mathbf{C}) = 2\frac{\partial \gamma_{\Gamma_0^a}(\mathbf{C})}{\partial \mathbf{C}} = \frac{1}{\Gamma_0^a}\frac{\partial U^{(a)}(\mathbf{C})}{\partial \mathbf{r}}\frac{\partial \mathbf{r}}{\partial \mathbf{C}}. \quad (12)$$

The surface Piola-Kirchoff stresses differ from those in the bulk because the normalization factor is an area, instead of a volume. In addition, the surface Piola-Kirchoff stresses $\widetilde{\mathbf{S}}^{(a)}$ $\times (\mathbf{C})$ are 3×3 tensors with normal components which allow surface relaxation due to undercoordinated atoms lying at material surfaces; this result differs from the traditional definition of surface stress[8] which is a 2×2 tensor with only tangential components.

The normal components arise in the present approach because the atoms that constitute the surface unit cells lack proper atomic coordination in the direction normal to the surface; therefore, the atomistic forces that are normalized to stresses in Eq. (12) are also out of balance in the normal direction. Thus, surface relaxation is necessary in the normal direction to regain an equilibrated state. Further details on the numerical implementation of the surface layers can be found in Ref. 48.
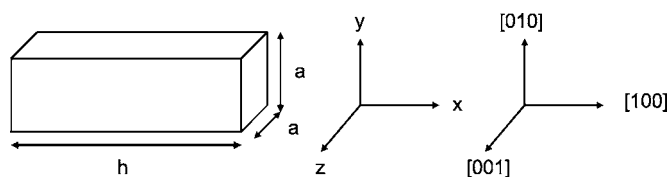
FIG. 2. Nanowire geometry considered for surface-stress-driven relaxation examples.

III. NUMERICAL EXAMPLES

All numerical examples presented have geometries similar to that shown in Fig. 2, which illustrates a gold nanowire with square cross section of length a and longitudinal length h. All wires had a $\langle 100 \rangle$ longitudinal orientation with $\{100\}$ transverse side surfaces, and were subject to the same boundary conditions; the left $(-x)$ surface of the wires were fixed, while the right $(+x)$ surface of the wires were constrained to move only in the x direction. All simulations, both molecular statics (MS) for the benchmark atomistics and the FE for the surface CB (SCB) were performed using the stated boundary conditions without additional external loading and without periodic boundary conditions. Therefore, all deformation observed in the examples is caused by the effects of surface stresses. All SCB calculations utilized regular meshes of eight-node hexahedral elements.

The atomistic interactions were based on the EAM, with gold being the material for all problems using the parameters of Foiles,[56] while the same parameters were used to calculate the bulk and surface stresses needed for the SCB simulations; single crystal gold nanowires were considered in all cases. Care was taken to consider nanowires with sizes large enough such that surface-stress-driven phase transformations[9] or reorientations,[57] which have been predicted in gold nanowires with cross sections smaller than about 2 nm, did not occur. We note that such inelastic deformation could be accommodated using nonlocal atoms, for example, following the example of the quasicontinuum method,[33] though this would require full atomistic resolution along the nanowire surfaces.

In the present work, the FE stresses were calculated using Eq. (4), while the tangent moduli were calculated using the numerical approximation of Miehe.[58] All simulations, for both FE and MS, were performed quasistatically to find energy minimizing positions of either the atoms or the FE nodes accounting for the surface stresses.

A. Direct surface Cauchy-Born and molecular statics comparison

The first example illustrates a direct comparison between a benchmark MS calculation and a SCB calculation. For this, the gold nanowire was comprised of 145 261 atoms with dimensions of 24.48 nm $\times$ 9.792 nm $\times$ 9.792 nm. The equivalent SCB model contained a regular mesh of 576 finite elements and 833 nodes, leading in a 99.4% reduction in the number of degrees of freedom; because similar mesh densities were used for all simulations shown in this work, similar reductions in the required degrees of freedom for the SCB calculations were achieved in all cases.
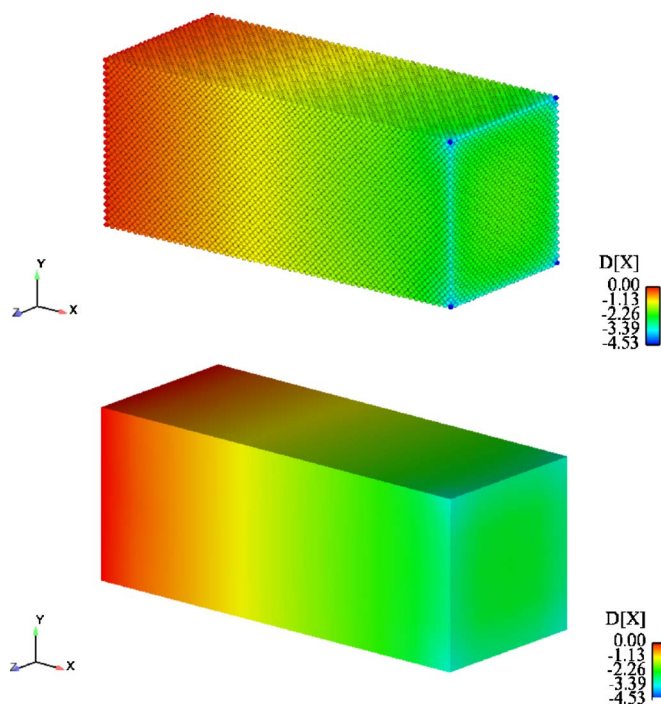

FIG. 3. (Color online) Comparison of x displacements for 24.48 nm $\times$ 9.792 nm $\times$ 9.792 nm gold nanowire for (top) MS and (bottom) SCB calculations.

Due to the surface stresses, the $+x$ edge of the wire contracts upon relaxation, resulting in an overall state of compressive strain in the wire. For both the MS and SCB calculations, the compressive strain was calculated by measuring the displacement at the center of the $+x$ surface at $(+x,0,0)$. This was done because, as seen in Fig. 3, the corners of the $+x$ surface of the nanowire have a greater contraction than the center of the $+x$ surface because they have the greatest degree of undercoordination. The SCB calculation predicted a compressive strain to relaxation of -0.91%, while the MS calculation predicted a contraction of -0.83%.

The fact that the SCB can predict the compressive relaxation is strengthened by comparative calculations for the relaxed and unrelaxed surface energy for both the SCB and MS systems for the same EAM potential; the unrelaxed surface energies γ_{ur} were found to be 0.975 J/m^2 for the MS system, and 0.973 J/m^2 for the SCB system for the $\{100\}$ surface of gold using Foiles *et al.*[56] potential. The relaxed surface energies γ_r were found to be 0.914 J/m^2 for the MS system, and 0.932 J/m^2 for the SCB system; the slight overestimation of the relaxed surface energy by the SCB correlates correctly with the higher relaxation strain in the above numerical example. Given the accuracy of the surface energy calculations, other sources of error between the SCB and MS simulations will be discussed later in the context of the numerical calculations.

The overall contours of the x and y displacements are shown in Figs. 3 and 4. As can be seen, the SCB calculations reproduce well the displacement fields in both the x and y directions, including the compressive relaxation in the x direction at the $+x$ edge of the nanowire, which then causes expansion of the nanowire in the y and z directions. The y
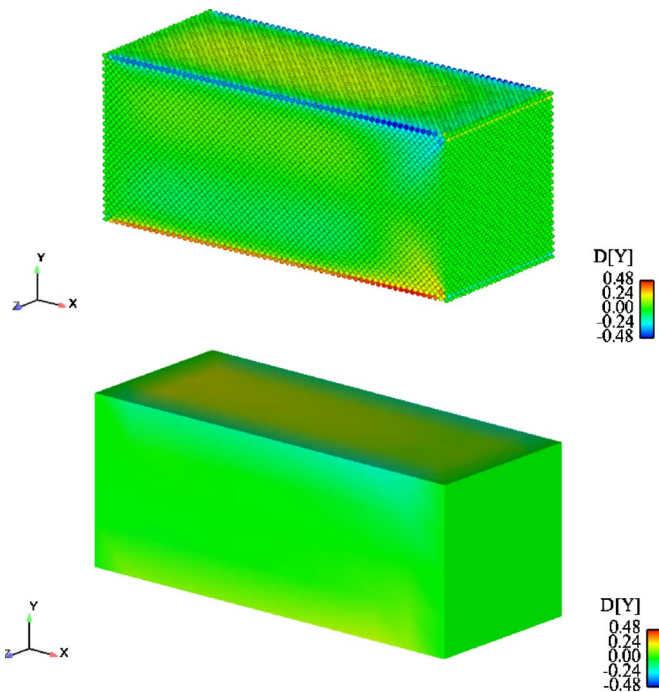
FIG. 4. (Color online) Comparison of y displacements for 24.48 nm×9.792 nm×9.792 nm gold nanowire for (top) MS and (bottom) SCB calculations.

displacement was calculated at the center of the $+y$ surface at $(0, +y, 0)$ and was compared for both the SCB and MS calculations; the SCB predicted an expansion of 0.18% while the MS calculation predicted an expansion of 0.17%.

The snapshots of the x and y displacements shown in Figs. 3 and 4 serve to highlight both the strengths and the weaknesses of the current version of the SCB method. As mentioned above, the SCB method clearly captures in a qualitative sense the overall relaxed configuration for the gold nanowire, at a greatly reduced computational cost as compared to the MS simulation. On the other hand, the results of the MS simulations show that the corners and edges of the nanowire experience a considerably different deformation than the surfaces and the bulk. Because the SCB method as currently formulated does not account for corner and edge effects, the deformation of those areas is captured in an average sense due to the deformation of the adjacent surfaces.

B. Parametric studies

1. Constant nanowire cross sectional area

Having analyzed the performance of the SCB model in the previous set of numerical examples, we now study the effects of the surface area to volume ratio along with nanostructure geometry using both the benchmark MS and SCB calculations. For the first set of simulations, a constant square cross section of length a was used, while systematically increasing the longitudinal length h. The MS calculations had a constant cross section of $a = 4.08$ nm, while the SCB calculations had square cross sectional lengths of $a = 5.72$, 8.7, and 16 nm; all wires with constant cross section

a were considered with lengths h between one and 16 times a. The smaller cross section for the MS calculations was considered due to computational expense. The number of atoms for the MS calculations ranged between 9041 and 70 781, while between 125 (for a 5.7 nm×5.7 nm×5.7 nm nanowire) and 20 817 (for a 512 nm×16 nm×16 nm nanowire) FE nodes were used.

By keeping the cross sectional area constant, the surface area (calculated as $2a^2 + 4ah$) to volume (calculated as a^2h) ratio tends to a constant value if h becomes large enough. For the MS case, the surface area to volume ratio approaches 0.98 nm^{-1}, while the ratios approach 0.025, 0.046, and 0.07 nm^{-1} for the $a = 16$, 8.7, and 5.72 nm cases, respectively. We analyzed variations in the compressive relaxation strain as the surface area to volume ratio approaches the limiting value; again, the compressive relaxation strain was calculated using the displacement at the center of the $+x$ surface at the point $(+x, 0, 0)$.

The results are summarized graphically in Fig. 5, which shows the compressive relaxation strain plotted versus normalized longitudinal length, where the normalization was by the smallest longitudinal length h_0 for a given cross sectional length a, and again versus surface area to volume ratio. Figure 5 captures several key features. First, as the nanowire length increases for a given cross sectional area, the amount of relaxation reduces nonlinearly to a limiting value at infinite length. In addition, the SCB calculations capture the fact that, for wires with smaller cross sections, the amount of relaxation strain initially increases at a higher rate for smaller normalized longitudinal lengths than for wires with larger cross sections; this is observed in Fig. 5(a). Also noteworthy is the fact that the larger cross section wires relax less for the same normalized lengths, thus correctly capturing the well-known behavior that surface stresses have a decreasing effect with increasing nanostructural size.

Finally, despite the variation in surface area to volume ratio for the different nanowires considered, all show the same linear relationship in Fig. 5(b) where the relaxation strain increases with decreasing surface area to volume ratio. The slopes of the surface to volume versus strain curves in Fig. 5(b) are 0.17 for the MS, and 0.12, 0.14, and 0.15 for the SCB with $a = 5.72$, 8.7, and 16 nm, respectively. The higher accuracy of the SCB calculations for the larger wires is likely due to the diminished effect of corners and edges at those length scales;[59] however, the results still show qualitative agreement in all cases.

2. Constant nanowire length

Simulations were also performed using the SCB model in which energy minimizing configurations of wires with a constant length of $h = 34.8$ nm and varying square cross sectional length from $a = 5.8$ to 34.8 nm under the influence of surface stresses were determined; the FE mesh sizes ranged from 625 to 15 625 nodes. The results are summarized in Fig. 6, and show two notable trends. First, as shown in Fig. 6(a), the SCB calculations predict that the equilibrium compressive strain is a nonlinear function of cross sectional area that increases rapidly for small cross sectional areas, while saturating to a limiting value for larger cross sectional areas; the
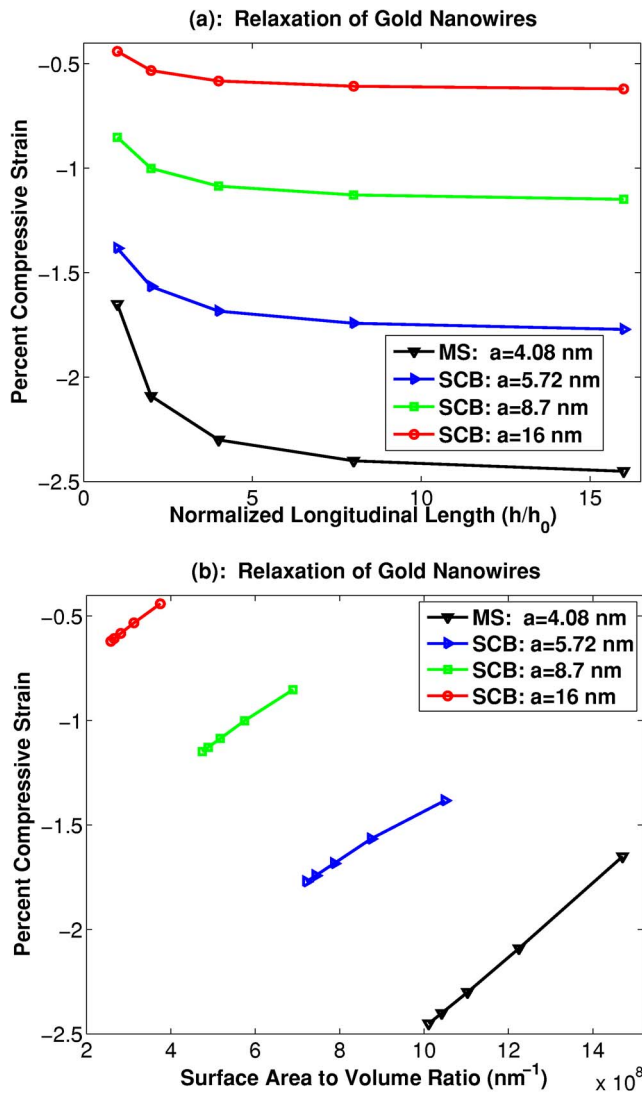
FIG. 5. (Color online) MS and SCB relaxation results for nanowires with constant square cross sectional lengths a, increasing longitudinal lengths h. (a) Strain as a function of normalized longitudinal length h_0. (b) Strain as a function of surface area to volume ratio.

FIG. 6. Relaxation results using the SCB method for gold nanowires with constant length of $h = 34.8$ nm with varying cross sectional area. (a) Strain versus normalized cross sectional length. (b) Strain versus surface area to volume ratio.

normalization is done by the smallest cross sectional length considered, $a_0 = 5.8$ nm.

More interestingly as illustrated in Fig. 6(b), the relaxation strain *increases* with increasing surface area to volume ratio. This is in stark contrast to the previous results in Fig. 5(b) considering nanowires with constant cross sectional areas with increasing lengths, where the relaxation strain *decreases* with increasing surface area to volume ratio. Thus, these results indicate that the surface area to volume ratio, which has been well documented[21] as playing a critical role in determining the unique mechanical properties of nanomaterials, cannot be utilized alone to predict minimum energy configurations for nanomaterials. Clearly, the geometry of the material must also be considered to make accurate predictions on minimum energy configurations.

The reason why longer wires tend to contract more than shorter wires even though they have a smaller surface area to
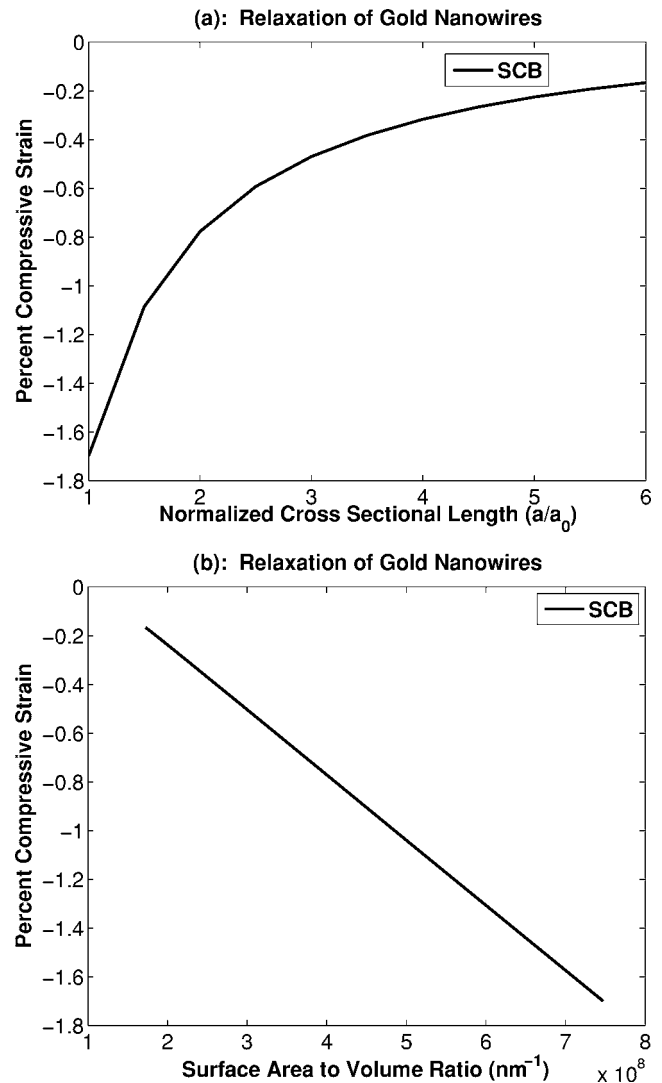
volume ratio is because they have a larger ratio of transverse ($4ah$) to total ($4ah + 2a^2$) surface area. Thus, longitudinal contraction allows the wire to efficiently reduce its exposed transverse surface area; the relevance of this point will be made clearer in the next section.

An analogy can be drawn here to recent work[10,11,22] on metal nanowires that has shown that $\langle 100 \rangle / \{100\}$ nanowires can reorient to $\langle 110 \rangle$ nanowires with $\{111\}$ transverse surfaces, which allows the nanowire to reduce its overall potential energy by exposing close packed and thus low energy $\{111\}$ transverse surfaces. While the SCB simulations do not allow such reorientations and were performed on large wires that are not expected to show the reorientation, they do capture the basic physics of transverse surface area reduction by increased relaxation strain for longer wires.

3. Constant surface area to volume ratio

Finally, simulations were performed using the SCB model on nanowires with the same surface area to volume ratio, but

different lengths and square cross sections. The wires considered all had a surface area to volume ratio of 0.28 nm^{-1}, square cross sections with lengths ranging from a =14.5 to 34.8 nm, and longitudinal lengths ranging from h =12 to 290 nm; the FE mesh sizes ranged from 3757 to 24 321 nodes. The compressive relaxation strains plotted against normalized area are shown in Fig. 7; the normalization factors are a_0 for Fig. 7(a), which is the smallest cross sectional length for all geometries considered, and the smallest surface area for all geometries considered for Fig. 7(b). As can be seen, the relaxation observed by wires with different geometries but the same surface area to volume ratio is not the same. For wires with the same surface area to volume ratio but different geometries, Fig. 7(b) illustrates that the cross sectional area can be strongly correlated to the relaxation strain.

Figure 7(b) illustrates conclusively that arguments based on *total* surface area reduction also cannot be utilized to predict the minimum energy configurations for nanowires with the same surface area to volume ratio. Instead, there appears to be a crossover point between −0.23% (where h < a) and −0.32% (where h > a) as labeled in Fig. 7(b), which corresponds to an estimate of the relaxation observed by a cubic wire with h=a. For nanowires that are much longer than wide (i.e., increasing h), the argument for surface area reduction holds and the wires show larger contractive strains. However, for nanowires whose cross sectional dimensions exceed the length (i.e., h < a), the wires show reduced contraction though the surface area increases as seen in Fig. 7(b).

The reason for this is shown in Fig. 7(c), which shows the relaxation strain plotted against the ratio of the transverse surface area, defined as $4ah$, to the total surface area of $4ah+2a^2$, and Table I, which summarizes the behavior of all wires with the same surface area to volume ratio. Both figures show that longer wires relax more longitudinally because they have the largest percentage of transverse surface area to reduce. Eventually, as the wire geometries become increasingly square and even pancakelike when h < a, the percentage of transverse surface area decreases and the driving force to contract longitudinally to reduce the exposed transverse surface area decreases as well, resulting in decreased relaxation.

The transverse surface area argument can also be used to understand the results seen for the two cases of wires considered earlier. The percentage of transverse surface area also explains the increasing relaxation for the wires in Fig. 5(b), which showed greater relaxation despite the decreasing surface area to volume ratio; again, making longer wires with the same cross sectional dimensions increases the percentage of transverse surface area, leading to increased relaxation. This also explains the trends seen in Fig. 6(b), in which wires with constant length and increasing cross sectional areas showed decreasing amounts of relaxation along with decreasing surface area to volume ratio; increasing the cross sectional dimensions keeping the length fixed decreases the percentage of transverse surface area, thus reducing the driving force for relaxation.
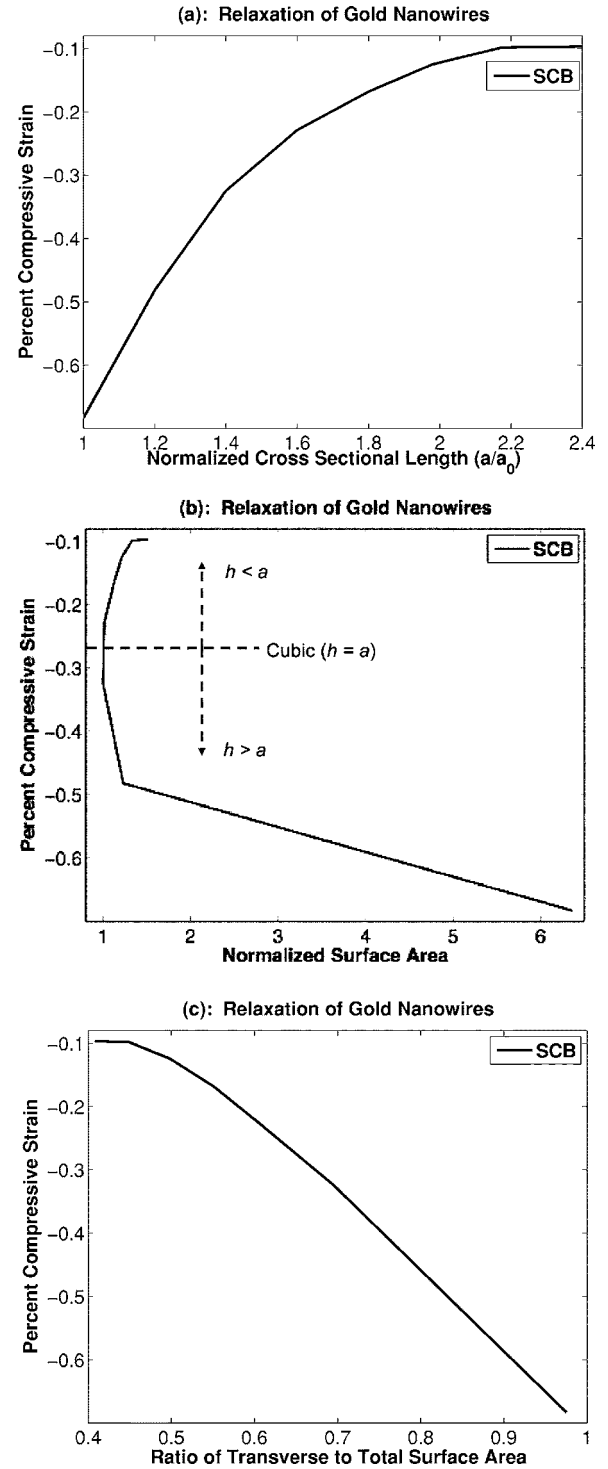

FIG. 7. Relaxation results using the SCB method for gold nanowires with the same surface area to volume ratio. (a) Strain versus normalized cross sectional length. (b) Strain versus normalized surface area. (c) Strain versus ratio of transverse to total surface area; ratio=$4ah/(2a^2+4ah)$.

IV. CONCLUSIONS

In this paper, we have developed a simple extension to the standard Cauchy-Born rule to capture surface stress effects on the mechanical behavior of single crystal FCC metallic

TABLE I. Summary for all wires with same surface area to volume ratio.

Wire size (nm)	Normalized surface area (nm^2)	Surface area to volume ratio (nm^{-1})	Ratio of transverse to total surface area: $4ah/(4ah+2a^2)$	Relaxation strain
$290 \times 14.5 \times 14.5$	6.37	0.28	0.98	-0.68%
$39.15 \times 17.4 \times 17.4$	1.23	0.28	0.82	-0.48%
$23.2 \times 20.3 \times 20.3$	1.0	0.28	0.70	-0.32%
$18 \times 23.2 \times 23.2$	1.01	0.28	0.61	-0.23%
$16 \times 26.1 \times 26.1$	1.12	0.28	0.55	-0.17%
$14.3 \times 28.7 \times 28.7$	1.21	0.28	0.50	-0.12%
$12.87 \times 31.5 \times 31.5$	1.33	0.28	0.45	-0.099%
$12 \times 34.8 \times 34.8$	1.51	0.28	0.41	-0.097%

nanostructures. The extension decomposes the total energy into bulk and surface components; the surface energy is then calculated using the Cauchy-Born approximation. The resulting potential energy can be minimized numerically using standard nonlinear finite element techniques, endowing the numerical model with the effects of the nanoscale surface stresses. Importantly, the surface Cauchy-Born model was shown to allow accurate predictions of the coupled effects of surface stress, size, and geometry on three-dimensional FCC metal nanostructures at low computational cost.

Numerical simulations using the proposed surface Cauchy-Born model have revealed the following: (1) The surface area to volume ratio alone cannot be utilized to predict minimum energy configurations for metal nanostructures. (2) Ideas based on total surface area minimization are also not sufficient to predict minimum energy configurations. (3) Just as geometry has been seen to greatly affect other physical properties of nanostructures,[60] the mechanical behavior of nanowires are found to be strongly geometry dependent;[61] long and slender wires, due to having a higher percentage of transverse surface area, will contract more in compression due to surface stresses than short and thick wires, which have a lower percentage.

It should be emphasized that some simulations were performed on wires with dimensions on the order of hundreds of nanometers, with cross sectional lengths on the order of tens of nanometers; future research investigating the mechanical properties of such nanowires will allow direct contact with recent experimental results on gold nanowires of similar size.[17] In addition, because the potential energy is minimized using finite elements, the approach can easily be used to model nanostructures with faceted geometries. In contrast, the method currently cannot be used to model phase transformations or surface reconstructions.

Finally, recent work has indicated that the modulus of nanowires is dependent upon the amount of compressive relaxation strain they undergo due to surface stresses.[21] The results obtained in this work have shown how wires with different geometries and surface area to volume ratios undergo different amounts of surface-stress-driven relaxation; correlation of this relaxation to modulus will be made in future work.

ACKNOWLEDGMENT

*Electronic address: harold.park@vanderbilt.edu

[1] S. Iijima, Nature (London) **354**, 56 (1991).

[2] L. T. Canham, Appl. Phys. Lett. **57**, 1046 (1990).

[3] C. M. Lieber, MRS Bull. **28**, 486 (2003).

[4] Y. Xia, P. Yang, Y. Sun, Y. Wu, B. Mayers, B. Gates, Y. Yin, F. Kim, and H. Yan, Adv. Mater. (Weinheim, Ger.) **15**, 353 (2003).

[5] C. R. Martin, Science **266**, 1961 (1994).

[6] M. Brust, M. Walker, D. Bethell, D. Schriffin, and R. Whyman, J. Chem. Soc., Chem. Commun. **7**, 801 (1994).

[7] Y. Arakawa and H. Sakaki, Appl. Phys. Lett. **40**, 939 (1982).

[8] R. C. Cammarata, Prog. Surf. Sci. **46**, 1 (1994).

[9] J. Diao, K. Gall, and M. L. Dunn, Nat. Mater. **2**, 656 (2003).

[10] H. S. Park, K. Gall, and J. A. Zimmerman, Phys. Rev. Lett. **95**, 255504 (2005).

[11] W. Liang, M. Zhou, and F. Ke, Nano Lett. **5**, 2039 (2005).

[12] H. S. Park, Nano Lett. **6**, 958 (2006).

[13] Y. Kondo and K. Takayanagi, Phys. Rev. Lett. **79**, 3455 (1997).

[14] Y. Kondo, Q. Ru, and K. Takayanagi, Phys. Rev. Lett. **82**, 751 (1999).

[15] E. W. Wong, P. E. Sheehan, and C. M. Lieber, Science **277**, 1971 (1997).

[16] S. Cuenot, C. Frétigny, S. Demoustier-Champagne, and B. Nysten, Phys. Rev. B **69**, 165410 (2004).

[17] B. Wu, A. Heidelberg, and J. J. Boland, Nat. Mater. **4**, 525 (2005).

[18] G. Y. Jing, H. L. Duan, X. M. Sun, Z. S. Zhang, J. Xu, Y. D. Li,

J. X. Wang, and D. P. Yu, Phys. Rev. B **73**, 235409 (2006).

[19] L. G. Zhou and H. Huang, Appl. Phys. Lett. **84**, 1940 (2004).

[20] V. B. Shenoy, Phys. Rev. B **71**, 094104 (2005).

[21] H. Liang, M. Upmanyu, and H. Huang, Phys. Rev. B **71**, 241403(R) (2005).

[22] H. S. Park, K. Gall, and J. A. Zimmerman, J. Mech. Phys. Solids **54**, 1862 (2006).

[23] M. E. Gurtin and A. Murdoch, Arch. Ration. Mech. Anal. **57**, 291 (1975).

[24] F. H. Streitz, R. C. Cammarata, and K. Sieradzki, Phys. Rev. B **49**, 10699 (1994).

[25] R. E. Miller and V. B. Shenoy, Nanotechnology **11**, 139 (2000).

[26] D. E. Segall, S. Ismail-Beigi, and T. A. Arias, Phys. Rev. B **65**, 214109 (2002).

[27] L. H. He, C. W. Lim, and B. S. Wu, Int. J. Solids Struct. **41**, 847 (2004).

[28] P. Sharma, S. Ganti, and N. Bhate, Appl. Phys. Lett. **82**, 535 (2003).

[29] C. T. Sun and H. Zhang, J. Appl. Phys. **92**, 1212 (2003).

[30] R. Dingreville, J. Qu, and M. Cherkaoui, J. Mech. Phys. Solids **53**, 1827 (2005).

[31] G. Wei, Y. Shouwen, and H. Ganyun, Nanotechnology **17**, 1118 (2006).

[32] J. Wang, H. L. Duan, Z. P. Huang, and B. L. Karihaloo, Proc. R. Soc. London, Ser. A **462**, 1355 (2006).

[33] E. Tadmor, M. Ortiz, and R. Phillips, Philos. Mag. A **73**, 1529 (1996).

[34] L. E. Shilkrot, R. E. Miller, and W. A. Curtin, J. Mech. Phys. Solids **52**, 755 (2004).

[35] J. Fish and W. Chen, Comput. Methods Appl. Mech. Eng. **193**, 1693 (2004).

[36] P. A. Klein and J. A. Zimmerman, J. Comput. Phys. **213**, 86 (2006).

[37] F. F. Abraham, J. Broughton, N. Bernstein, and E. Kaxiras, Europhys. Lett. **44**, 783 (1998).

[38] R. E. Rudd and J. Q. Broughton, Phys. Rev. B **58**, R5893 (1998).

[39] W. E and Z. Y. Huang, J. Comput. Phys. **182**, 234 (2002).

[40] G. J. Wagner and W. K. Liu, J. Comput. Phys. **190**, 249 (2003).

[41] H. S. Park, E. G. Karpov, W. K. Liu, and P. A. Klein, Philos. Mag. **85**, 79 (2005).

[42] H. S. Park, E. G. Karpov, and W. K. Liu, Comput. Methods Appl. Mech. Eng. **193**, 1713 (2004).

[43] S. P. Xiao and T. Belytschko, Comput. Methods Appl. Mech. Eng. **193**, 1645 (2004).

[44] W. K. Liu, E. G. Karpov, and H. S. Park, *Nano Mechanics and Materials: Theory, Multiscale Methods and Applications* (Wiley, New York, 2006).

[45] X. Li and W. E, J. Mech. Phys. Solids **53**, 1650 (2005).

[46] W. K. Liu, E. G. Karpov, S. Zhang, and H. S. Park, Comput. Methods Appl. Mech. Eng. **193**, 1529 (2004).

[47] T. Belytschko, W. K. Liu, and B. Moran, *Nonlinear Finite Elements for Continua and Structures* (Wiley, New York, 2002).

[48] H. S. Park, P. A. Klein, and G. J. Wagner, Int. J. Numer. Methods Eng. **68**, 1072 (2006).

[49] P. A. Klein, Ph.D. thesis, Stanford University, 1999.

[50] M. Arroyo and T. Belytschko, J. Mech. Phys. Solids **50**, 1941 (2002).

[51] M. S. Daw and M. I. Baskes, Phys. Rev. B **29**, 6443 (1984).

[52] P. Zhang, Y. Huang, P. H. Geubelle, P. A. Klein, and K. C. Hwang, Int. J. Solids Struct. **39**, 3893 (2002).

[53] E. B. Tadmor, G. S. Smith, N. Bernstein, and E. Kaxiras, Phys. Rev. B **59**, 235 (1999).

[54] Y. Zhao and B. I. Yakobson, Phys. Rev. Lett. **91**, 035501 (2003).

[55] T. J. R. Hughes, *The Finite Element Method: Linear Static and Dynamic Finite Element Analysis* (Prentice-Hall, New york, 1987).

[56] S. M. Foiles, M. L. Baskes, and M. S. Daw, Phys. Rev. B **33**, 7983 (1986).

[57] J. Diao, K. Gall, and M. L. Dunn, Phys. Rev. B **70**, 075413 (2004).

[58] C. Miehe, Comput. Methods Appl. Mech. Eng. **134**, 223 (1996).

[59] J. Q. Broughton, C. A. Meli, P. Vashishta, and R. K. Kalia, Phys. Rev. B **56**, 611 (1997).

[60] K. L. Kelly, E. Coronado, L. L. Zhao, and G. C. Schatz, J. Phys. Chem. B **107**, 668 (2003).

[61] C. Ji and H. S. Park, Appl. Phys. Lett. **89**, 181916 (2006).